Two-Dimensional Model for Circulating Fluidized-Bed Reactors

H. Schoenfelder, M. Kruse, and J. Werther
Dept. of Chemical Engineering, Technical University Hamburg-Harburg, D-21071 Hamburg, Germany

A two-dimensional reactor model for circulating fluidized beds (CFB) was studied based on the assumption that at every location within the riser, a descending dense phase and a rising lean phase coexist. Fluid mechanical variables may be calculated from one measured radial solids flux profile (upward and downward). The internal mass-transfer behavior is described on the basis of tracer gas experiments. The CFB reactor model was tested against data from ozone decomposition experiments in a CFB cold flow model (15.6-m height, 0.4-m ID) operated in the ranges 2.5–4.5 m/s and 9–45 kg/(m^2·s) of superficial gas velocity and solids mass flux, respectively. Based on effective reaction rate constants determined from the ozone exit concentration, the model was used to predict the spatial reactant distribution within the reactor. Model predictions agreed well with measurements.

Introduction

Circulating fluidized bed reactors are widely used for the combustion of coal in power stations as well as for the cracking of heavy oil in the petroleum industry. Moreover, a number of new applications such as the production of maleic anhydride (Contractor et al., 1993) or the combustion of sewage sludge and other waste material (Werther et al., 1995) can be expected for the near future. Reactor models for circulating fluidized beds have undergone a development from rather simple approaches assuming plug flow (e.g., Van Swaaij, 1978) or dispersed plug flow (Edwards and Avidan, 1986) of gas toward more complex descriptions of the system. Most state-of-the-art circulating fluidized-bed reactor models (Kagawa et al., 1991; Schoenfelder et al., 1994b; Basu et al., 1994) make use of the core/annulus approach, which dates back to the work of Brereton et al. (1988). The principle of these models is to assume two phases to exist in the riser at every axial location, an upward moving dilute phase (core) and a dense phase (annulus) with high solids concentrations and either stagnant or slowly downward flowing gas. These one-dimensional two-phase approaches can account for two major characteristics of circulating fluidized bed reactors: bypassing and backmixing of gas. Thus, these models yield a quantitative description of the gas/solid contact efficiency, which may be significantly lower than in the case of plug flow of gas.

The one-dimensional core/annulus models have reached a reasonable degree of maturity. They have been applied to a number of small-scale installations. However, it is uncertain at the moment whether it is possible to use this type of model for scale-up. A major problem is the lack of information about the influence of the reactor diameter on the mass transfer between core and annulus. Moreover, there is a significant contradiction between the assumption of a distinct core/annulus interface in the riser and experimental data never showing a steplike change of different variables along the riser radius. Such a strict core/annulus boundary was found neither with respect to the local solids flux (Rhodes et al., 1992), nor the local solids concentration (Zhang et al., 1991), nor the local gas velocity (Horio et al., 1996), nor the distribution of continuously injected tracer gas (Kruse et al., 1995), nor the concentration of different species in a circulating fluidized bed combustor (Boemer et al., 1993). Recent experimental work by Ouyang et al. (1993) has demonstrated that there are distinct spatial profiles of the reactant concentration for the ozone decomposition reaction even in a riser of only 0.254 m in diameter. Particularly for the large-scale circulating fluidized-bed combustors, it is probable that three-dimensional models may be necessary for the application in industry. The results of such a three-dimensional model for circulating fluidized-bed combustors have been presented by Tsuo et al. (1995). Unfortunately, most of the details of the model are proprietary.

Correspondence concerning this article should be addressed to J. Werther.
Present address of: H. Schoenfelder, BASF AG, D-67056, Ludwigshafen, Germany; M. Kruse, Dietrich Reimelt KG, D-63322 Rödermark, Germany.

In two previous publications (Kruse and Werther, 1995; Kruse et al., 1995), a two-dimensional two-phase gas-mixing model for the upper dilute zone has been suggested that is based on the assumption that at every location within the riser two phases coexist: a descending dense phase (representing downfalling clusters) and an ascending lean phase (representing upflowing dilute suspension). Contrary to the core/annulus approach, the two phases may occur at the same location in the riser at different times. The probability of the occurrence of the dense phase is described by its time-averaged local volume fraction, f_d, which is assumed to be a function of both radial and axial position in the riser. The dependence of f_d on the radial position is described by a power-law function. Its parameters as well as other fluid mechanical variables are calculated from one pair of measured profiles of local solids flux (upward and downward). The model has successfully demonstrated its ability to describe the complex gas-mixing behavior of the circulating fluidized bed riser with respect to the distribution of tracer gas that was continuously injected over the circumference of the riser.

In this article we report on the development of a two-dimensional reactor model for circulating fluidized beds, which makes use of the gas-mixing model described earlier. The model has been tested with the ozone decomposition as a model reaction. This reaction system has been used successfully by other authors in the field (Van Swaaij et al., 1972; Ouyang et al., 1993, 1995). The experiments have been carried out in the same circulating fluidized bed system that was used for the gas-mixing experiments. Thus, the numerical values of the model parameters could be taken from the previous investigation (Kruse et al., 1995).

Modeling

Axial staging

In the case of risers for catalytic reactions, many authors treat the flow of gas and solids as fully developed (Pugsley et al., 1992). On the other hand, systems operated under conditions closer to those of circulating fluidized bed combustors definitely require consideration of the different flow structures near the gas distributor and in the upper part of the riser (Arena et al., 1991; Schoenfelder et al., 1994b; Basu et al., 1994). In the present investigation, the riser is subdivided axially into two different zones, the bottom zone and the upper dilute zone. As indicated in Figure 1, the axial solids concentration profile determines the extension of the two zones.

In the present study, there is no definition of a splash zone to separate the bottom zone from the upper dilute zone. Instead, the bottom zone is assumed here to include that part of the riser where descending clusters from the upper dilute phase are decelerated and dissolved into the upflowing suspension. The decision where to set the interface between the two zones is taken according to a measured solids concentration profile based on pressure differential measurements.

Modeling the upper dilute zone

In two previous publications the authors have presented a two-dimensional model to describe the behavior of the upper dilute zone with respect to flow structure (Kruse and Werther, 1995) and gas mixing (Kruse et al., 1995). Since the reaction model presented in this article is an extension of these previous approaches, only brief descriptions are given here.

A Model for the Flow Structure in the Upper Dilute Zone. The view of the flow structure that the model is based on is shown in Figure 2. It is assumed that at every location in the upper dilute zone, dense clusters of particles may appear. By definition, these clusters move downward, countercurrently to the upflowing lean suspension that surrounds them. The terms *dense phase* and *lean phase* are used to denote clusters and lean suspension. The local volume fraction, f_d, of the dense phase is assumed to vary with axial and radial position in the riser. The solids of the dense phase move downward with a velocity v_d. Since reactant gas is captured within the falling clusters, their motion causes a backmixing of gas. The interstitial velocity of the downward moving gas in the dense phase is called u_d. For calculation of u_d, it is assumed that the relative velocity between gas and solids in the dense phase obeys the correlation of Richardson and Zaki (1954). As well as both dense phase velocities, v_d and u_d, the dense phase solids volume fraction, c_{vd}, is assumed to be invariant with radial position. The lean phase interstitial gas velocity, u_l, is assumed to be a function of both radial and axial position in

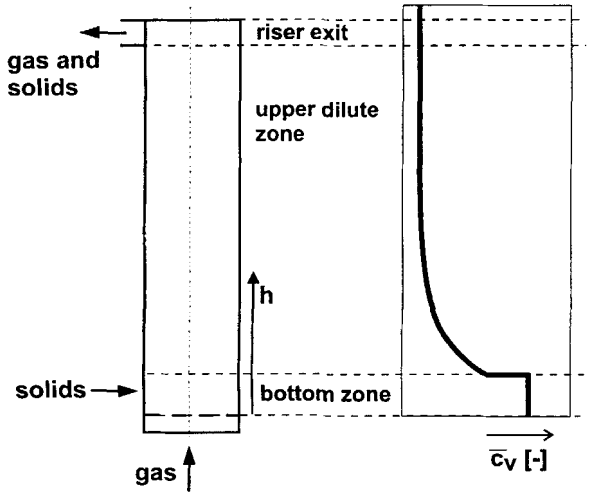

Figure 1. Axial subdivision of the CFB riser according to the solids concentration profile.

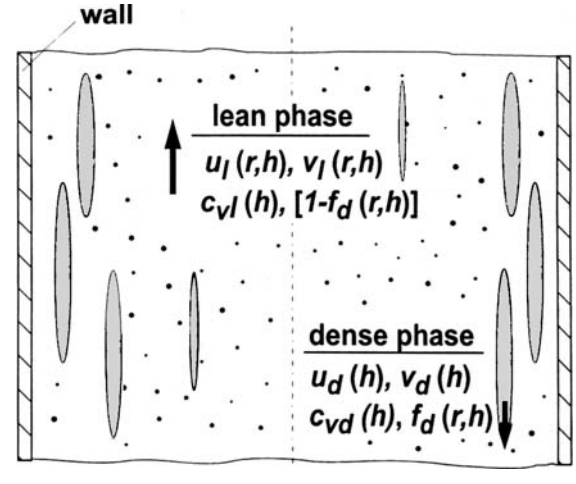

Figure 2. Flow structure in the upper dilute zone of the circulating fluidized bed riser.

the riser. The solids in the lean phase move relatively to the upflowing gas with the terminal settling velocity of the single particle. The absolute solids velocity of the lean phase is called v_l, and the lean phase solids concentration is referred to as c_{vl}, which is assumed to be invariant with the radial position.

The description of the flow structure in the upper dilute zone is complete, if the values of all of the variables introduced earlier are known at every radial and axial position in the riser. For their determination, a method has been presented in a previous publication (Kruse and Werther, 1995). Its principle and some simplifications for the present study are described in the following.

The method is based on the assumption that the dependence of f_d on the radial position can be described with a simple power law function:

$$f_d = f_{dw}\left(\frac{r}{R}\right)^m, \tag{1}$$

where the parameter f_{dw} has to be determined for every axial position. The other parameter, m, is characteristic for a given system and assumed constant. As can easily be seen from Eq. 1, the approach assumes that no downfalling clusters occur in the centerline of the riser, whereas a maximum concentration of the dense phase is found adjacent to the riser wall.

An analysis of the data given by Kruse et al. (1995) shows that the dense phase solids fraction, c_{vd}, can be estimated from the cross-sectional averaged solids volume fraction as

$$c_{vd}(h) = \bar{c}_v(h)^{0.57}. \tag{2}$$

This finding corresponds well to the results of Lints and Glicksman (1992), who have found the correlation $c_{vd} = \bar{c}_v^{0.5}$ to yield a good description of experimental data from various researchers.

In the present study, the axial profile of the cross-sectional averaged solids concentration, $\bar{c}_v(h)$, is described in the upper dilute zone with the exponential decay function suggested by Kunii and Levenspiel (1991),

$$\bar{c}_v = \bar{c}_{v\infty} + (\bar{c}_{v'} - \bar{c}_{v\infty})e^{-a(h-H_b)}. \tag{3}$$

In the present study, all parameters of Eq. 3 were fitted to experimental data obtained from pressure differential measurements. The influence of acceleration and friction on the pressure profiles is neglected.

The key feature of the approach is a method to calculate radial profiles of the upward and downward solids fluxes [$G_{sl}(r, h)$ and $G_{sd}(r, h)$] for given operating conditions at every axial position in the riser. As input data for the calculation one measured pair of radial profiles of $G_{sl}(r, H_m)$ and $G_{sd}(r, H_m)$ at a height H_m is required. The experiments can be carried out at reference conditions (u_{ref}, $G_{s,\text{ref}}$) that must not necessarily be identical with those for which the flow structure has to be calculated. The method extends the concept of similar profiles of solids net fluxes, which was discovered by Monceaux et al. (1986) and confirmed by other authors (e.g., Molodtsof, 1992; Rhodes et al., 1992), to the profiles of the upward and downward solids flux, respectively. In an experimental investigation (Kruse and Werther, 1995), it was found that at a given axial position in the developed flow region of the riser the reduced profiles of upward and downward solids flux [$G_{sl}(r)/G_s$ and $G_{sd}(r)/G_s$] are insensitive toward changes of gas velocity and solids circulation rate. It can therefore be stated that they are characteristic of the riser geometry and the properties of the gas/solids system.

The measured radial profiles of upward and downward solids mass fluxes are described by power-law functions. The approach for solids downflow follows from Eq. 1, using the assumption of a constant dense phase solids velocity v_d at a given height h:

$$\frac{G_{sd}}{G_s}(r) = F\left(\frac{r}{R}\right)^m, \tag{4}$$

where F, the maximum reduced solids downward flux at the riser wall, is constant for all operating conditions at a given height.

In the previous study (Kruse and Werther, 1995), the local solids flux was found to vary with the axial position in the riser. For a given operating state, the reduced downward solids flux was found to be proportional to $\bar{c}_v(h)$. Based on this finding, Eq. 5 was developed as a means of calculating all radial profiles of local downward solids flux as a function of the axial position, h:

$$\frac{G_{sd}}{G_s}(h,r) = \bar{c}_v(h)D\left(\frac{r}{R}\right)^m \qquad D = \frac{F(H_m)}{\bar{c}_v(H_m)}, \tag{5}$$

where parameter D is constant for a given set of operating conditions at any height within the riser.

In the present study, upflow of particles at the riser wall is neglected. Thus, the following equation is proposed to represent the radial profile of local upward solids flux:

$$\frac{G_{sl}}{G_s} = A\left[1-\left(\frac{r}{R}\right)^n\right], \tag{6}$$

where n is constant for all operating conditions at all axial positions in a given system and A may be calculated for any height from the condition that the integral of the reduced solids flux has to equal unity,

$$A(h) = \left(\frac{1}{2} - \frac{\bar{c}_v(h)D}{m+2}\right)\left(2+\frac{4}{n}\right). \tag{7}$$

The parameters F, m, n are constant for all operating conditions at a given height. For their determination, one measured pair of radial profiles of upward and downward local solids flux is analyzed. F and m are obtained from the measured local downward solids flux profile by fitting. The parameter n is then calculated by fitting Eq. 6 to the measured radial profile of local upward solids flux.

In order to calculate the local profiles of upward and downward solids flux for a given set of operating parameters at any axial location in the upper dilute zone, the following steps have to be performed:

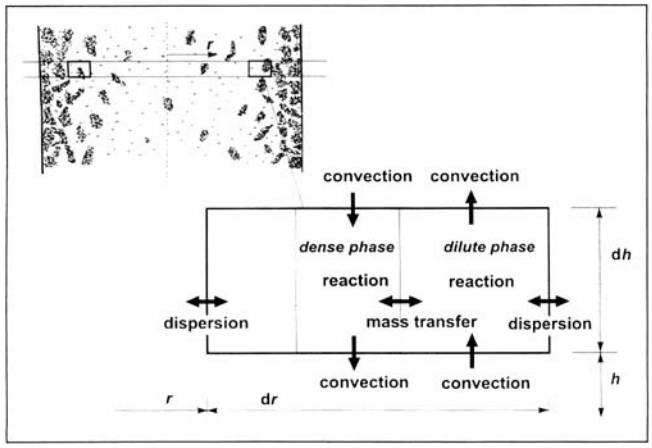

Figure 3. Mass balance for a differential volume in the upper dilute zone.

1. Measurement of a pair of radial profiles of local upward and downward solids flux profiles in the given CFB system (geometry, gas, solids) under reference conditions (u_{ref}, $G_{s,\mathrm{ref}}$) at a height H_m. Fitting calculations yield F, m, and n.

2. Calculation or measurement of axial solids concentration profile, $\bar{c}_v(h)$ for operating conditions of interest (u, G_s). Calculate D as $D = F/\bar{c}_v(H_m)$.

3. Calculate radial profiles of local upward and downward solids fluxes at any height in the upper dilute zone for operating conditions (u, G_s), using Eqs. 5, 6, and 7.

Once the radial profiles of local upward and downward solids fluxes are determined, local and integral mass balances for gas and solids may be used to calculate the characteristic properties, that is, u_l, c_{vl}, v_l, f_d, u_d, c_{vd}, v_d. More details have been given by Kruse and Werther (1995).

Reaction Behavior in the Upper Dilute Zone. In order to obtain a two-dimensional description of the behavior of the upper dilute zone with respect to chemical reactions, mass balances for the chemical species are formulated for a differential volume element of the upper dilute zone. The element depicted in Figure 3 has the volume $2\pi r\,dr\,dh$.

In this volume element, two different phases, dense and lean, coexist and exchange gas with each other. Transport of gas in the axial direction is convective in both phases, downward in the dense phase and upward in the lean phase, and axial dispersion is neglected. Whereas for gas in the lean phase it is assumed that radial transport occurs by dispersion, this effect is neglected for the dense phase. Transport of gas by adsorption on the particles is neglected. Chemical reactions are considered in the dense as well as in the lean phase. In the present state of development, the model can only be applied to reactions that do not cause a change of the molar gas flux. Moreover, the catalyst activity in the reactor is assumed to be uniform.

Figures 4 and 5 show differential volume elements in the upper dilute zone of the dense and lean phase, respectively, including all terms of the mass balances. Note that all variables for the description of the flow structure as well as their spatial derivatives are known from the preceding calculation of the flow structure. It can be performed independently from the description of the reaction behavior, because the chemical reactions are assumed not to affect the flow structure.

The flow conditions are changing with height in the upper

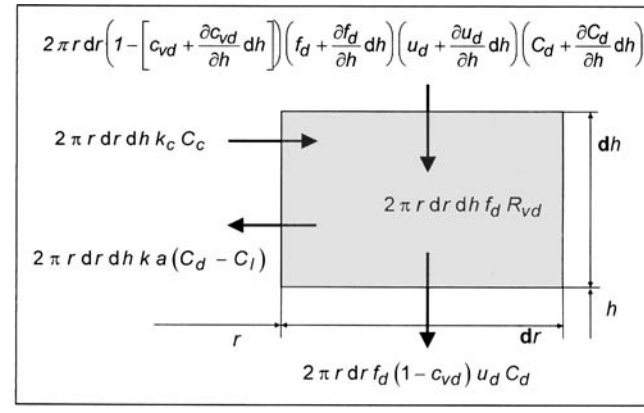

Figure 4. Mass balance for a differential control volume of the dense phase.

dilute zone. In particular the dense phase volume fraction, f_d, is decreasing with height. This requires the introduction of a convective exchange between the dense and the lean phase (characterized by k_c) and a radial gas velocity, u_r. The convective exchange flux per unit reactor volume, k_c, may be calculated from a balance of the volumetric gas flow for the differential volume of the dense phase, cf. Figure 4,

$$k_c(r,h) = \left(u_d\frac{\partial f_d}{\partial h} + f_d\frac{\partial u_d}{\partial h}\right)(1-c_{vd}) - \frac{\partial c_{vd}}{\partial h}f_d u_d. \quad (8)$$

Note that the concentration of the gas that is either transferred into the dense or into the lean phase, C_c, is a function of the direction of the convective flux

$$C_c = \begin{cases} C_l, & \text{for } k_c > 0 \\ C_d, & \text{for } k_c < 0. \end{cases} \quad (9)$$

The radial gas velocity, u_r, is calculated from a balance of the volumetric gas flow for the differential volume of the dense phase, cf. Figure 5,

$$\frac{\partial u_r}{\partial r} = -\frac{u_r}{r} - k_c + \frac{\partial f_d}{\partial h}u_l(1-c_{vl}) + \frac{\partial c_{vl}}{\partial h}u_l(1-f_d) - \frac{\partial u_l}{\partial h}(1-f_d-c_{vl}+c_{vl}f_d). \quad (10)$$

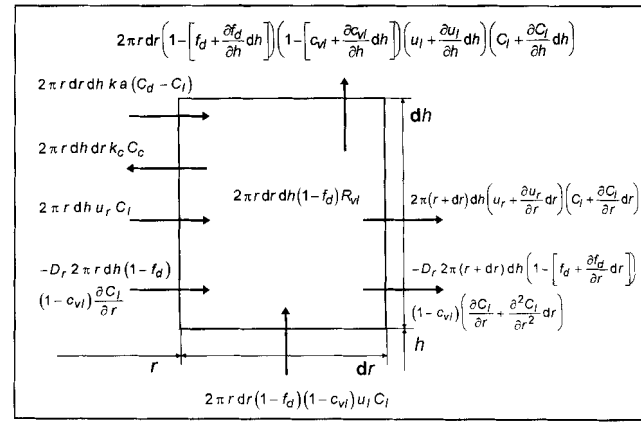

Figure 5. Mass balance for a differential control volume of the lean phase.

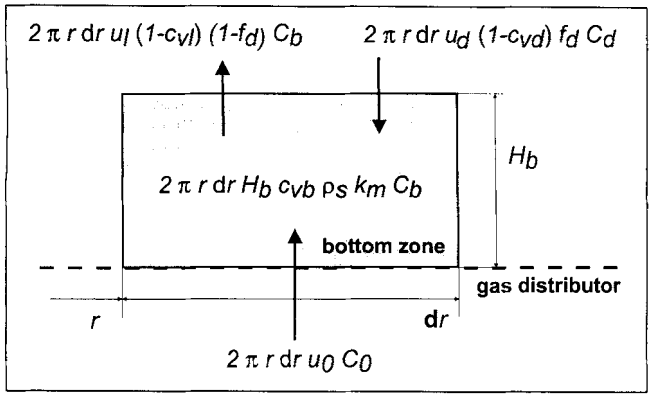

Figure 6. Mass balance for a volume of differential radius in the bottom zone of the riser.

The differential equation is solved with the boundary condition at the riser wall $u_r(r = R) = 0$.

The mass exchange between the dense and the lean phase is characterized by the product $k \cdot a$ of a mass transfer coefficient, k (based on the unit mass transfer area), and the volume-specific mass transfer area, a. The mass transfer area between the phases will certainly be influenced by the local volume fraction of the dense phase, f_d. If we consider a single cluster to have a surface area based on its volume, a^*, a amounts to $a^* f_d$. If the number of clusters (and thus f_d) increases, the value of a will also increase until coalescence of the clusters will again reduce the mass transfer area. In the case $f_d = 1$, no mass transfer area would be available. The approach used here to describe the dependence of a on f_d is formulated as $a = a^* f_d(1 - f_d)$. Thus, the resulting expression for $k \cdot a$ is

$$k \cdot a = k^* f_d (1 - f_d), \tag{11}$$

where k^* may be understood as the mass exchange coefficient of a single downfalling cluster. In our previous study (Kruse et al., 1995), a value of $k^* =$ about 0.3 s^{-1} has been determined for sand particles in a rather dilute circulating fluidized bed system, where values of f_d were low and the approximation $k \cdot a = k^* f_d$ was used. In order to avoid parameter fitting, the value of $k^* = 0.3$ s^{-1} is assumed to be valid for all operating conditions in the present study, too. The cluster size is thus assumed not to vary with the operating conditions.

The radial dispersion coefficient, D_r, was determined experimentally in the preceding study (Kruse et al., 1995) for the same circulating fluidized bed riser that is used here. The result was presented in the form of the Peclet number, Pe_r, which was found to be constant throughout the range of operating conditions investigated:

$$Pe_r = \frac{u d_t}{D_r} = 387. \tag{12}$$

Though the solids system of the present study is different from that used in the former investigation, as a first approximation the resulting value of $Pe_r = 387$ is assumed to be valid.

In this investigation, the reaction rate of the regarded species, R_v, describes the catalytic decomposition of ozone. Since this is a first-order reaction (Van Swaaij and Zuiderweg, 1972), the expression for the reaction rate is rather simple

$$R_{vd} = c_{vd}\, \rho_s k_m C_d \tag{13a}$$

$$R_{vl} = c_{vl}\, \rho_s k_m C_l \tag{13b}$$

where the reaction rate constant, k_m, is defined per unit catalyst mass.

In Figures 4 and 6, the vectors of the convective dense phase fluxes point downward in order to provide a better illustration of the flow structure. With all vectors pointing in the positive direction of the axial coordinate, h, the resulting differential equation for the reactant concentration in dense phase can easily be derived from the balance as

$$\begin{aligned} 2\pi r dr\left(1-\left[c_{vd}+\frac{\partial c_{vd}}{\partial h}dh\right]\right)\left(f_d+\frac{\partial f_d}{\partial h}dh\right)\left(u_d+\frac{\partial u_d}{\partial h}dh\right) \\ \times\left(C_d+\frac{\partial C_d}{\partial h}dh\right)-2\pi r dr f_d(1-c_{vd})u_d C_d \\ +2\pi r dr dh k a(C_d - C_l) \\ -2\pi r dr dh k_c C_c - 2\pi r dr dh f_d R_{vd} = 0. \end{aligned} \tag{14}$$

The corresponding lean-phase partial differential equation is

$$\begin{aligned} 2\pi r dr\left(1-\left[f_d+\frac{\partial f_d}{\partial h}dh\right]\right)\left(1-\left[c_{vl}+\frac{\partial c_{vl}}{\partial h}dh\right]\right)\left(u_l+\frac{\partial u_l}{\partial h}dh\right) \\ \times\left(C_l+\frac{\partial C_l}{\partial h}dh\right)-2\pi r dr(1-f_d)(1-c_{vl})u_l C_l \\ -2\pi r dr dh k a(C_d - C_l) - D_r 2\pi dr dh(1-c_{vl}) \\ \times\left(r\frac{\partial^2 C_l}{\partial r^2}(1-f_d)+\frac{\partial C_l}{\partial r}(1-f_d)-r\frac{\partial C_l}{\partial r}\frac{\partial f_d}{\partial r}\right) \\ +k_c 2\pi r dr dh C_c + 2\pi dr dh\left[\frac{\partial u_r}{\partial r}r C_l + u_r\left(\frac{\partial C_l}{\partial r}r + C_l\right)\right] \\ -2\pi r dr dh(1-f_d)R_{vl} = 0. \end{aligned} \tag{15}$$

The partial differential equation, Eq. 15, is solved using the following boundary conditions in the radial direction:

$$r = 0: \qquad \frac{\partial C_l}{\partial r} = 0 \tag{16a}$$

$$r = R: \qquad \frac{\partial C_l}{\partial r} = 0. \tag{16b}$$

In the axial direction, two boundary conditions for the solution of the differential equations, Eqs. 14 and 15, are given at both ends of the riser. At the lower end of the upper dilute zone, the boundary condition for the lean phase is simply given by the gas concentration of the bottom zone

$$h = H_b: \qquad C_l = C_b, \tag{17}$$

where C_b is calculated from a bottom zone model, which is described in the following section. For the dense phase, which is moving in the downward direction, the adequate boundary condition is not as obvious. A good agreement with the experimental results is obtained if we assume that at the riser exit all axial gradients of the dense-phase concentrations are vanishing,

$$h = H_t: \qquad \frac{\partial C_d}{\partial h} = 0. \tag{18}$$

Bottom-zone modeling

Unfortunately, there is not enough experimental knowledge about the phenomena near the gas distributor in a circulating fluidized bed available to allow detailed two-dimensional modeling of the bottom zone. Instead, we are restricted to a rather rough approach.

The solids volume concentration in the bottom zone, c_{vb}, is assumed to be invariant with vertical and horizontal position. Its numerical value is determined by the overall pressure balance of the riser,

$$c_{vb} = \frac{\Delta p}{H_b g \rho_s} - \frac{1}{H_b}\int_{H_b}^{H_t} \bar{c}_v(h)dh. \tag{19}$$

In Eq. 19 it is assumed that acceleration and friction effects on the local pressure drop are negligible.

In order to describe the behavior of the bottom zone with respect to the two-dimensional gas mixing behavior we make the following assumptions:

1. As proposed by Luca et al. (1995), gas mixing in the axial direction is assumed to be complete.
2. Gas mixing in the radial direction is assumed to be complete for $r > R_{\text{net}}$, where R_{net} denotes the location of zero net flow of solids in the upper dilute zone at $h = H_b$.
3. Gas mixing in the radial direction is negligible for $r < R_{\text{net}}$.
4. The local superficial gas velocity at the gas distributor level, $u_0(r)$, is related to the interstitial velocities in the two phases at the lower boundary ($h = H_b$) of the upper dilute zone by

$$u_0 = u_l(1-c_{vl})(1-f_d) + u_d(1-c_{vd})f_d. \tag{20}$$

The equation to calculate the concentration C_b in the bottom zone at a given radial position, r, can easily be derived from Figure 6. It holds that

$$C_b = \frac{u_0 C_0 - u_d(1-c_{vd})f_d C_d}{u_l(1-c_{vl})(1-f_d) - H_b c_{vb}\rho_s k_m}. \tag{21}$$

Since in the region $r > R_{\text{net}}$ the radial gas mixing is assumed to be complete, it holds for the reactant concentration in the wall region, C_{bw}, that,

$$C_{bw} = \frac{u_{0w}(R-R_{\text{net}})^2 C_0 - \int_{R_{\text{net}}}^{R} 2ru_d(1-c_{vd})f_d C_d dr}{\int_{R_{\text{net}}}^{R} 2ru_l(1-c_{vl})(1-f_d)dr - H_b(R-r_{\text{net}})^2 c_{vb}\rho_s k_m}, \tag{22}$$

where the average superficial gas velocity in the range $R > r > R_{\text{net}}$ at the gas distributor, u_{0w}, is calculated as

$$u_{0w} = \frac{\int_{R_{\text{net}}}^{R} 2ru_l(1-c_{vl})(1-f_d)dr + \int_{R_{\text{net}}}^{R} 2ru_d(1-c_{vd})f_d dr}{(R-R_{\text{net}})^2}. \tag{23}$$

Note that in Eqs. 20 to 23, all variables of the upper dilute zone have to be calculated for $h = H_b$. Due to the backmixing of gas from the dense phase of the upper dilute phase into the bottom zone, Eqs. 20 to 23 have to be solved simultaneously with the partial differential equations describing the upper dilute zone of the riser. In the solving algorithm used in the present study, the bottom-zone model is treated as a complex boundary condition for the upper dilute zone.

Solving algorithm

The system of partial differential equations is solved with the method of finite differences. A grid of 200(axial)$\times$ 20(radial) elements was found to allow for a sufficient calculation accuracy. Due to the linear behavior of the first-order ozone decomposition reaction, the method yields a system of $200\times20\times2$ linear equations, which was solved numerically using standard FORTRAN routines for band diagonal systems provided by Press et al. (1992). Computational times are of the order of 10 min on a 486/33 system.

Experimental

Circulating fluidized bed system

The CFB system used in the present study is depicted in Figure 7. The riser is 15.6 m high and has an internal diameter of 0.4 m. Solids separated from the gas stream by two cyclones are returned to the riser via a siphon. More details about the apparatus and the measuring techniques are given elsewhere (Hartge et al., 1988).

For the present investigation, an ozone generator (Hans Neumayer GmbH, Freiburg, Germany) was connected to the main air supply. The ozone was fed to the fluidizing air directly after the blower to allow for a sufficient mixing length before the gas enters into the windbox of the CFB riser. Thus, the ozone was completely mixed with the primary air at the gas distributor. The ozone concentration in the fluidizing air was adjusted to about 2 ppm.

Solids System. The catalyst used in the experiments is a porous amorphous aluminum hydrosilicate with about 10% of crystalline silica. A certain amount of iron oxide acts as active component for the decomposition of ozone. The material called K-306 is produced by Süd-Chemie AG, Munich. The solids apparent density is about 1,420 kg/m^3 (estimated from the bulk density with $\epsilon = 0.5$), and the minimum fluidization velocity of the used catalyst with a Sauter mean diameter of 50 μm was determined to be 1.9 10^{-3} m/s (ambient air, 20°C, 100 kPa). The particle-size distribution was measured every day during the measuring campaign. After an initial loss of fines, the particle-size distribution in the CFB system remained constant at values plotted in Figure 8.

The first-order reaction rate constant based on the unit

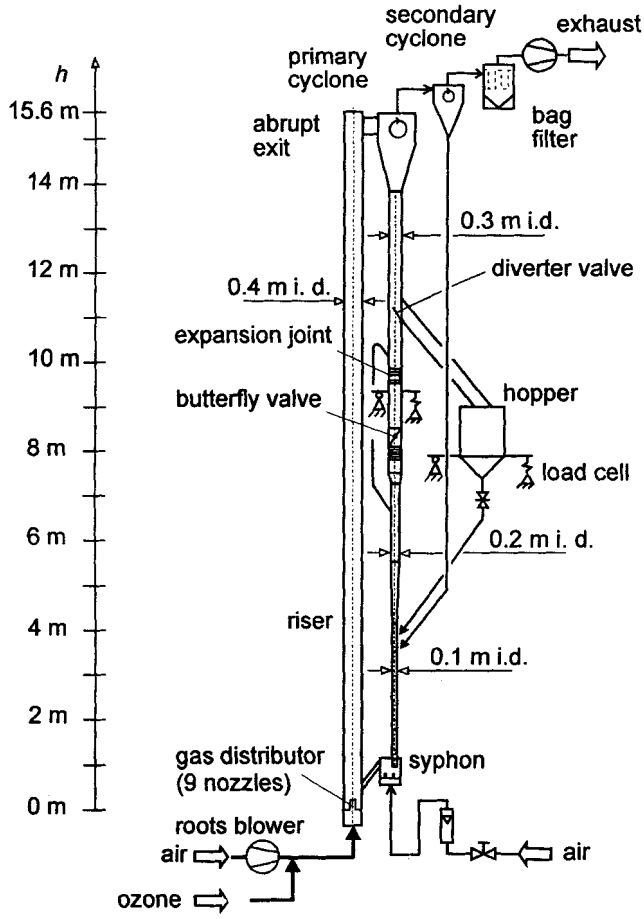

Figure 7. CFB system.

mass catalyst, k_m, was in the range of $-1.0\ 10^{-3}$ to $-3.0\ 10^{-3}$ m^3/(s·kg) for the conditions in the CFB riser. The value is strongly influenced by the temperature as well as by the moisture content of the fluidizing air (Van Swaaij and Zuiderweg, 1972). Therefore, no externally measured reaction-rate constants were used as input data for the modeling, and values of k_m were determined by fitting model calculations to the outlet concentration of ozone.

Local solids mass flux measurements

The model approach for the description of the flow structure in the CFB riser is based on one measurement of a pair of radial profiles of upward and downward solids mass flux. The measurements were carried out at a height of 8.4 m above the gas distributor.

A suction probe system as depicted in Figure 9 has been used to obtain the experimental data. The probe was especially designed for measuring local solids mass fluxes of fine and light particles. It was rotated to measure either the upward or downward solids fluxes. In order to be able to vary the suction velocity at the probe tip without the risk of blocking inside the conveying line, an internal recycle probe was designed following earlier work (Werther, 1993). The key feature of the design is an internal recirculation of air in the probe system, which allows low gas velocities at the probe tip and a sufficient conveying gas velocity after the recycle air injection (only 15 mm downstream the suspension inlet).

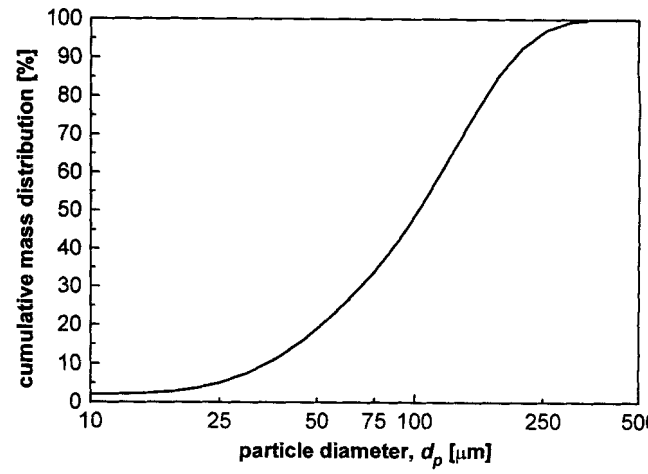

Figure 8. Particle size distribution of K-306 after 40 h of operation in the CFB system. (By laser analyzer, Sympatec GmbH, Clausthal, Germany.)

During the measurements, the probe was kept in suction operation for 30 s before the weight of solids in the collector was determined. The procedure was repeated twice and if the scattering of the three measurements exceeded 15%, a fourth measurement was carried out. Thus, a single data point is the average value of at least three separate measurements.

For fluidizing velocities between 2.5 and 4.5 m/s, an optimum suction velocity at the probe tip, u_{tip}, of about 0.7 m/s and a conveying velocity inside the probe of about 5 m/s were found in earlier calibration tests. Under these conditions, reproducible results with a minimum deviation between the external solids circulation rate and the integral of the net local solids flux were obtained. The deviation varied between +10% and +130%, which may be due to the very fine and light catalyst particles. The measured data were used in the form of the reduced solids mass flux profiles [$G_{sl}(r)/G_{si}$ and $G_{sd}(r)/G_{si}$], where G_{si} is calculated from the integral of the measured profiles. These reduced profiles are not too sensitive to errors of the absolute values of G_{sl} and G_{sd}.

Ozone concentration measurements

Gas samples from the CFB riser were continuously collected and analyzed by the experimental setup shown in Fig-

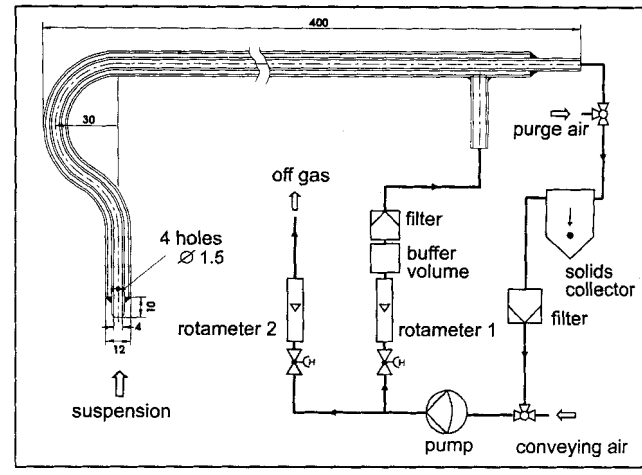

Figure 9. The suction probe system.

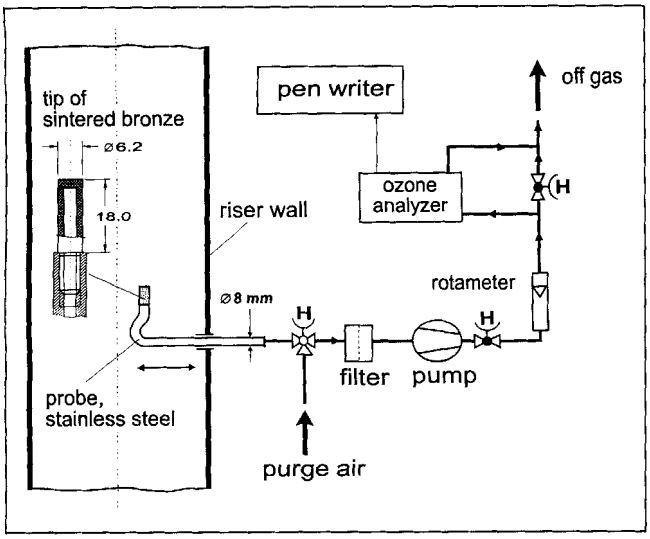

Figure 10. Experimental setup for ozone concentration measurements.

ure 10. The gas sampling probes are equipped with a cylindrical tip of sintered bronze with a length of 18 mm and an outer diameter of 6.2 mm. Solids retention of the sintered bronze with a pore diameter of about 10 μm was complete. An appropriate sealing mechanism allowed to adjust the measuring position of the probe in the radial direction during operation of the CFB.

A sampling pump with a Teflon membrane (ASF GmbH, Puchheim, Germany) is used to withdraw the gas from the CFB system. Tubes and valves that are in contact with the ozone-containing gas are made of Teflon to prevent unintended decomposition. The gas is transported to the ozone analyzer (Beckman Instruments Ltd., Fullerton, USA), which used the chemiluminescent reaction of ethene and ozone to formaldehyde as the measuring principle.

In an initial blank run, the decomposition of ozone in the empty tube of the CFB was measured. At all locations in the riser, the ozone concentration was found to lie in a range of

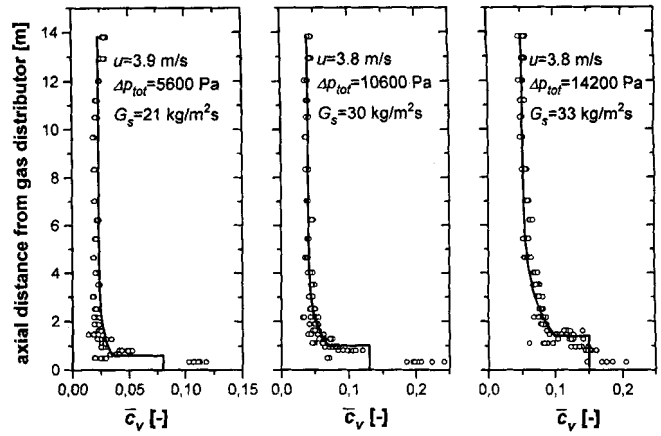

Figure 12. Axial solids concentration profiles (from pressure differential measurements) for u = about 3.75 m/s.

Symbols: experimental data from 7 separate measurements. Solid lines: best fit model calculation (Eqs. 3 and 19).

98.5–100% of the value measured below the gas distributor. Therefore, the effect of undesired decomposition of ozone was neglected.

In order to determine ozone concentration profiles, measuring ports at axial distances of 1.1, 3.1, 6.1, 9.1, and 13.1 m above the gas distributor were used to insert probes. Moreover, gas samples for measuring ozone concentrations were taken below the gas distributor and between the primary and secondary cyclone to yield information about the inlet and outlet concentration, respectively. Radial profiles of the ozone concentration were obtained from measurements at radial positions $r/R = 0$, 0.4, 0.6, 0.775, and 0.975. During an experimental run, all probes currently not in use were flushed by small amounts of purge air. The sampling gas of the probe in operation was fed to the analyzer until the steady-state signal was recorded for at least 1 min to measure the local ozone concentration, C. The desired measuring information used for the model evaluation is the local dimensionless ozone concentration, C/C_0. Therefore, the ozone concentration C_0 be-

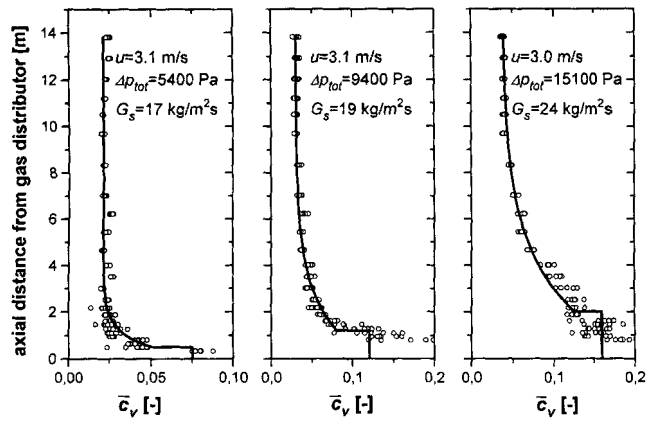

Figure 11. Axial solids concentration profiles (from pressure differential measurements) for u = about 3 m/s.

Symbols: experimental data from 7 separate measurements. Solid lines: best fit model calculation (Eqs. 3 and 19).

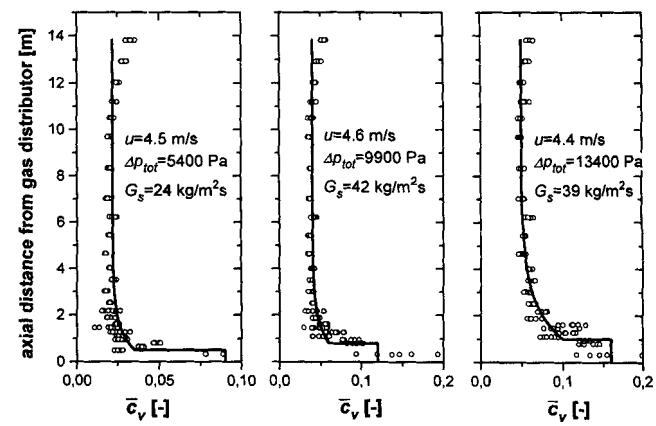

Figure 13. Axial solids concentration profiles (from pressure differential measurements) for u = about 4.5 m/s.

Symbols: experimental data from 7 separate measurements. Solid lines: best fit model calculation (Eqs. 3 and 19).

Table 1. ID-character, Operating Conditions, and Best-Fit Parameters of Axial Solids Concentration Profiles (Eqs. 3 and 19) of the Ozone Decomposition Measurements

ID	u m/s	Δp_{tot} Pa	G_s kg/(m²·s)	$\bar{c}_{v'}$	$\bar{c}_{v\infty}$	a m^{-1}	H_b m	c_{vb}
0	2.5	5,400	11	0.035	0.02	1	0.75	0.1
A	3.1	5,400	17	0.05	0.022	1.5	0.4	0.08
B	3.9	5,600	21	0.035	0.023	1	0.6	0.08
C	4.5	5,400	24	0.035	0.022	1	0.5	0.09
D	3.1	9,400	19	0.08	0.03	0.5	1.2	0.12
E	3.8	10,600	30	0.07	0.041	1	1	0.13
F	4.6	9,900	42	0.06	0.04	1	0.8	0.12
G	3.0	15,100	24	0.125	0.038	0.35	2	0.16
H	3.8	14,200	33	0.1	0.051	0.6	1.4	0.15
I	4.4	13,400	39	0.1	0.05	0.7	1	0.16

low the gas distributor was determined immediately before and after the measurement of an axial concentration profile using the probes from within the CFB riser.

Results and Discussion

Axial solids distribution

The experiments for the investigation of the ozone decomposition in the CFB system were carried out under ten different operating conditions. The gas velocity was adjusted within the range of 2.5–4.5 m/s and the total riser pressure drop was varied between 5,400 and 15,100 Pa. In Figures 11, 12, and 13 axial profiles of the cross-sectional averaged solids volume fraction, $\bar{c}_v(h)$, are plotted. Each plot contains experimental data from seven separate measurements that have been taken during an entire day of steady-state operation of the CFB system. It can be seen that in the case of low total riser pressure drop, that is, low solids holdup, the cross-sectional average solids concentration, $\bar{c}_v(h)$, is constant throughout almost the total height of the riser. On the other hand, when the solids holdup is high, a significant decay of $\bar{c}_v$ is found over almost the whole riser length. In the case of the highest gas velocity ($u = 4.5$ m/s) a slight exit effect, causing increasing solids concentrations at the riser top has been observed. The effect is neglected in the present study, but should be considered if the model is applied to a CFB system with an axial concentration profile that is significantly influenced by exit effects.

The measurements of the axial solids distribution were used to determine the parameters and results of Eqs. 3 and 19, respectively, in order to provide a mathematically usable basis for the modeling. Table 1 gives an overview of the operating conditions chosen for the ozone decomposition measurements as well as of the corresponding parameters of the axial solids distribution. Every operating state can be identified by an uppercase character that is listed in the first row of Table 1. The experimental conditions described in Table 1 can be divided into three groups with different total riser pressure drop, Δp_{tot}, of about 5,500, about 10,000, and about 14,000 Pa, respectively. Within each group the superficial gas velocities were adjusted to approximate values of 3, 3.75 or 4.5 m/s.

Local solids mass flux profiles and flow structure

In the previous section dealing with the flow structure, a calculation method is presented that can be applied to determine all variables of the two-dimensional description of the flow structure. This method is based on both the information given in the last section and a measured pair of radial profiles of reduced solids fluxes, G_{sl}/G_{si} and G_{sd}/G_{si}. An important advantage of the method is that the solids flux measurement must not necessarily be carried out at the same operating conditions that the model is used for. It was decided to use measurements at a medium gas velocity of 3.6 m/s as input data for the calculation. In Figure 14, the results of the measurement are depicted together with the best fit model calculations using Eqs. 4 and 6. The parameters were determined as $F = -2.7$, $n = 1.9$, and $m = 6.0$. These values are the basis of all model calculations presented in the following.

On the basis of the axial solids concentration profiles and the parameters F, n, and m, the method described earlier was used to calculate the parameters of the two-dimensional flow structure model for all operating conditions used in the ozone decomposition experiments. As an example, in Table 2 an overview of the parameter values of the model at a height of 12 m is given.

For each axial position in the riser, the radial distribution of the lean phase gas velocity, u_l, and the dense phase volume fraction, f_d, is calculated. Figures 15 and 16 show some examples of the model predictions. The radial profiles of the

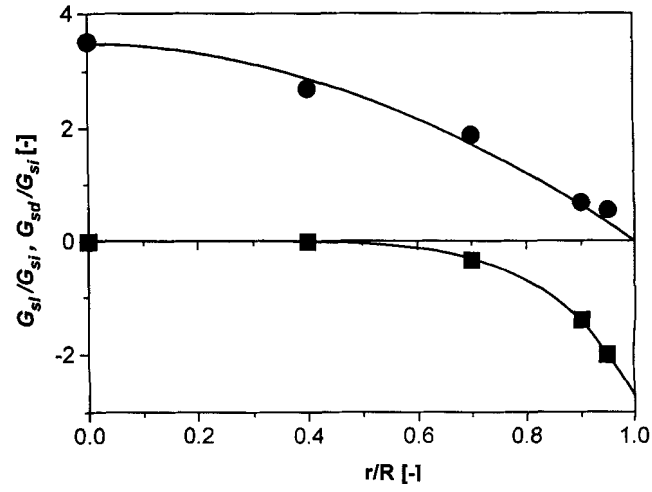

Figure 14. Radial profiles of reduced local solids mass flux.

Symbols: measured data at reference conditions [$u_{ref} = 3.6$ m/s, $G_{s,ref} = 24$ kg/(m²·s), $H_m = 8.4$ m]. Solid lines: model calculation using Eqs. 4 and 6 ($F = -2.7$, $n = 1.9$, and $m = 6.0$).

Table 2. Parameters of the Two-dimensional Description of the Flow Structure at the Operating States for the Ozone Decomposition Measurements at a Height of 12 m

ID	u m/s	Δp_{tot} Pa	G_s kg/(m^2·s)	$\bar{c}_{vl}$	$\bar{c}_{vd}$	v_d m/s	u_d m/s	f_{dw}
0	2.5	5,400	11	0.0052	0.10	−0.33	−0.26	0.60
A	3.1	5,400	17	0.0064	0.11	−0.47	−0.40	0.61
B	3.9	5,600	21	0.0064	0.11	−0.57	−0.50	0.63
C	4.5	5,400	24	0.0062	0.11	−0.68	−0.61	0.61
D	3.1	9,400	19	0.0073	0.13	−0.36	−0.30	0.73
E	3.8	10,600	30	0.0093	0.16	−0.42	−0.36	0.86
F	4.6	9,900	42	0.011	0.16	−0.65	−0.59	0.81
G	3.0	15,100	24	0.088	0.15	−0.30	−0.24	0.84
H	3.8	14,200	33	0.0086	0.18	−0.34	−0.29	0.99
I	4.4	13,400	39	0.010	0.18	−0.43	−0.38	0.97

dense-phase volume fraction in Figure 15 indicate that the descending dense phase is concentrated close to the riser wall. In contrast to the core-annulus approach, we see a monotonous decrease of the dense phase volume fraction with increasing distance from the wall. Increasing the solids holdup in the riser leads not only to an increase of f_d, but also to increased values of c_{vd} and c_{vl} (cf. Table 2). The plot of the lean-phase gas velocity, u_l, shows steep profiles that strongly deviate from the turbulent velocity profiles of the single-phase gas flow. Increasing the fluidizing velocity, u, leads to an even steeper profile.

The dependence of the u_l and f_d profiles on height above the distributor is shown in Figure 16. With increasing height above the distributor, the volume fraction of the dense phase is decreasing, which is due to the decrease of cross-sectional average solids volume fraction with height (cf. Figure 11). The different $f_d(r)$ profiles are reflected in the development of $u_l(r)$ with height.

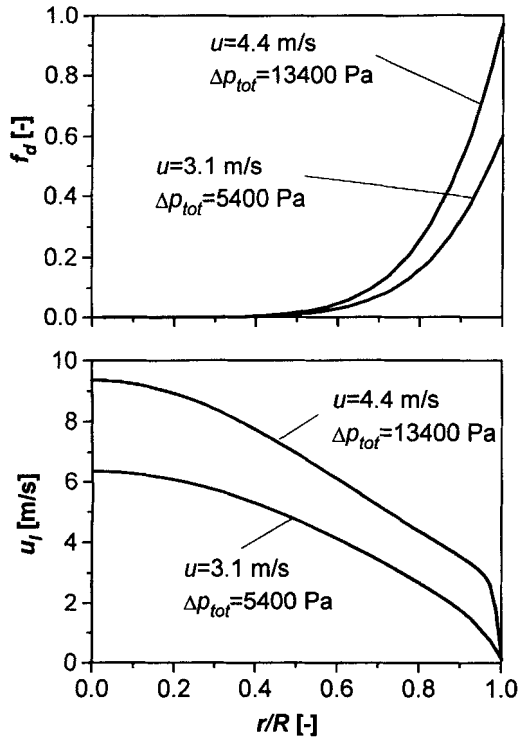

Figure 15. Comparison of calculated radial profiles of f_d and u_l for two different operating states [u=3.1 m/s, Δp_{tot}=5,400 Pa (ID: A) and u=4.4 m/s, Δp_{tot}=13,400 Pa (ID: I)] at a height of 12 m above the distributor.

Ozone concentration profiles

The results of the calculation of the fluid mechanical variables as described in the previous section are used as input data for the model of the reaction behavior of the CFB. In the following, the modeling results obtained as solutions of the system of differential equations, Eqs. 14 and 15, are compared to experimental data.

At a given location in the upper dilute zone of the riser, the results of the model calculation consist of two ozone concentration values: one for the lean and one for the dense phase. For comparing the model calculation with experimental data, it is assumed that the gas-sampling probe draws off

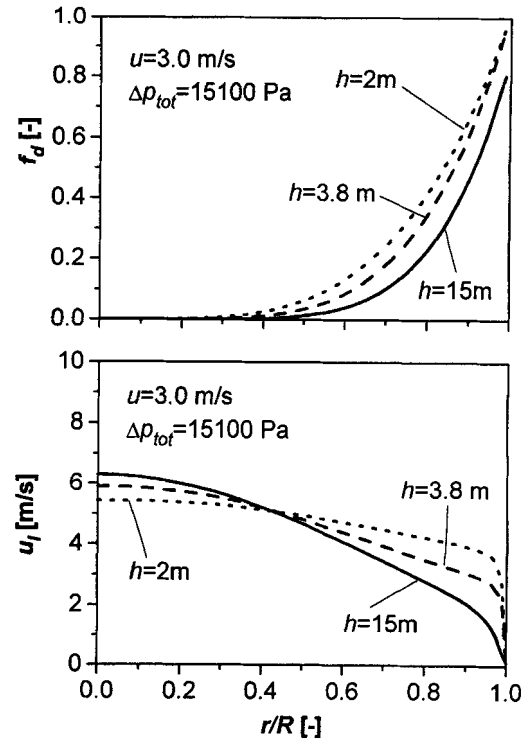

Figure 16. Comparison of calculated radial profiles of f_d and u_l for one operating state [u=3.0 m/s, Δp_{tot}=15,100 Pa (ID: G)] at different axial positions.

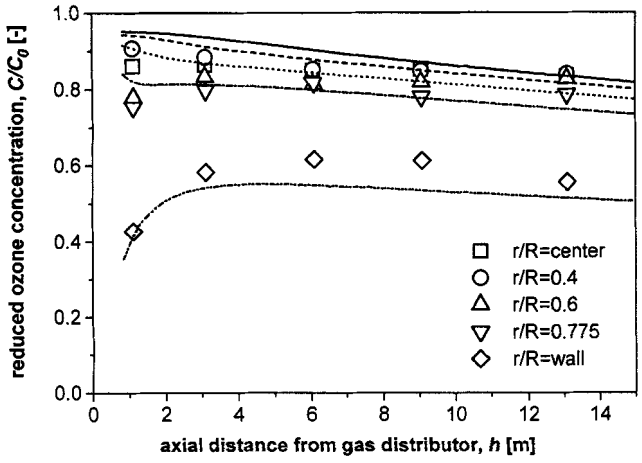

Figure 17. Comparison of calculated and measured ozone concentration profiles [$u = 2.5$ m/s, $\Delta p_{tot} = 5{,}400$ Pa, $G_s = 11$ kg/(m^2·s)].

Symbols: experimental data. Lines: model calculation [$k_m = -1.6 \times 10^{-3}$ kg/(m^2·s)].

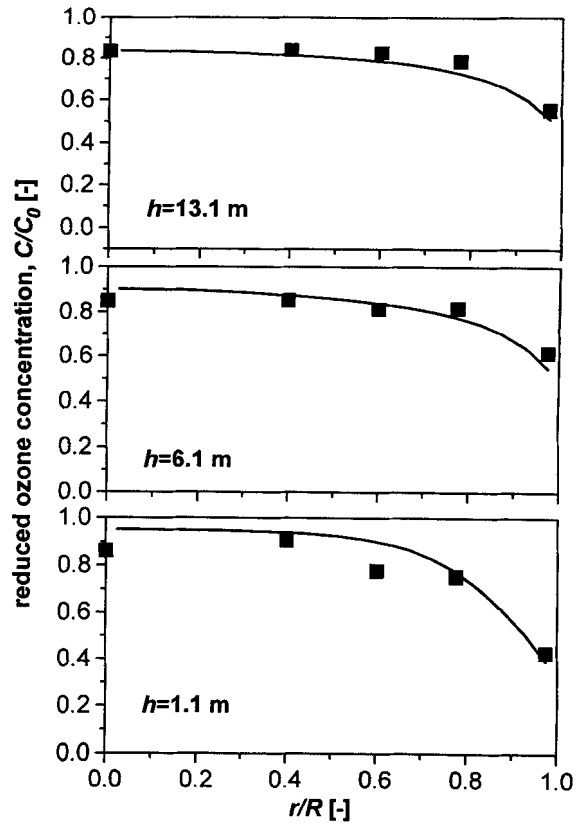

Figure 18. Comparison of three calculated and measured radial ozone concentration profiles [$u = 2.5$ m/s, $\Delta p_{tot} = 5{,}400$ Pa, $G_s = 11$ kg/(m^2·s)].

Symbols: experimental data. Lines: model calculation [$k_m = -1.6 \times 10^{-3}$ kg/(m^2·s)].

the gas from both phases and that the amount of gas originating from a phase is proportional to its local volume fraction. Thus, it holds for the local ozone concentration

$$C = C_d f_d + C_l(1 - f_d). \tag{24}$$

The model calculations require the reaction rate constant, k_m, as input parameter. Values of k_m were obtained by fitting the calculated outlet ozone concentration, C_{out}, which is obtained from integrating the local ozone concentrations in the upflowing lean phase at the axial position H_t

$$C_{out} = \frac{1}{R^2} \int_0^R C_l u_l (1 - f_d)(1 - c_{vl}) r dr \tag{25}$$

to the measured outlet concentration.

The reaction-rate constants being fixed, the model allows predictions of the spatial distribution of the reactant concentration inside the whole upper dilute zone of the riser. As an example, Figure 17 shows calculated and predicted axial profiles of the reduced ozone concentration, $C/C_0(h, r)$, at different radial positions.

It can be seen from Figure 17 that the ozone concentration in the centerline of the riser is almost constant with riser height, and only minor differences between the ozone concentration profiles at radial positions between $r/R = 0$ and $r/R = 0.775$ are found. Near the wall, on the other hand, a significantly lower ozone concentration has been measured. Here, a maximum of the ozone concentration is observed at a medium height above the gas distributor. This result corresponds well with earlier findings by Kagawa et al. (1991) and Ouyang et al. (1993, 1995), who have found qualitatively similar concentration profiles adjacent to the wall for the ozone decomposition reaction in smaller CFB systems. Figure 18 depicts some of the data presented in Figure 17 in the form of radial profiles of measured and calculated ozone concentration. The profiles are steep near the bottom zone and more flat at elevated positions in the riser.

Obviously, there is a good agreement between calculated and measured ozone concentration profiles in Figures 17 and 18. Even the slight maximum of the ozone concentration, which has been measured at the riser wall, is confirmed by the model. Some deviations occur near the bottom zone, which is due to the very rough model for the bottom zone.

In the same way as in the example of Figures 17 and 18, the model calculations have been performed for all experiments listed in Table 1. An overview of the outlet concentrations and the best fit reaction rate constants is given in Table 3.

Figure 19 compares measured and calculated ozone concentration profiles for the experiments that have been taken at low values of the solids holdup. The pressure drop over the whole riser length was about 5,500 Pa. In these and all following plots, the results for the radial position $r/R = 0.4$ have been omitted, because they are in all cases very close to the values in the centerline of the riser. The model predictions are again in good agreement with the measurements.

Figure 20 shows a similar comparison between measurements and predictions for three operating conditions that are characterized by riser pressure drops, Δp_{tot}, between 9,400 and 10,600 Pa. A comparison with Figure 19 reveals that the increasing solids holdup causes significantly higher ozone concentration differences between the centerline and the wall region of the system. Obviously, the model is very well able

Table 3. Measured Reduced Ozone Concentrations at the Riser Outlet and Best Fit Reaction Rate Constants

ID	u m/s	Δp_{tot} Pa	G_s kg/(m²·s)	C/C_0, Outlet	k_m m³/(kg·s)
0	2.5	5,400	11	0.78	-1.6×10^{-3}
A	3.1	5,400	17	0.84	-1.6×10^{-3}
B	3.9	5,600	21	0.82	-2.6×10^{-3}
C	4.5	5,400	24	0.85	-2.4×10^{-3}
D	3.1	9,400	19	0.71	-2.3×10^{-3}
E	3.8	10,600	30	0.77	-1.8×10^{-3}
F	4.6	9,900	42	0.76	-2.7×10^{-3}
G	3.0	15,100	24	0.72	-1.0×10^{-3}
H	3.8	14,200	33	0.69	-3.0×10^{-3}
I	4.4	13,400	39	0.73	-2.6×10^{-3}

to describe this behavior. The calculated axial concentration profiles in the centerline and at the wall are in good agreement with the measured data.

On the other hand, it is seen that there is a deviation between experimental and calculated data at the radial position of $r/R = 0.775$. In the cases depicted in Figure 20 the predicted ozone concentrations at this radial position are sometimes much higher than the measured values. This turns out to be a characteristic deviation, which is even more obvious from the plots given in Figure 21. It shows again a comparison between measurements and predictions for operating conditions that are characterized by high solids holdups. The total pressure drop in these plots were in the range 13,400–15,100 Pa.

When the solids holdup is increased, an obvious change of the shape of the ozone concentration profiles is observed. Whereas in the case of low values of the solids holdup the ozone concentration gradient at the riser wall is very high, the profiles become much smoother in the case of a higher solid holdup. This finding has also been reported by Ouyang et al. (1995), who have examined the ozone decomposition under similar conditions as in the present study. Evidently, the present model cannot fully account for the change of the reactor behavior at the radial position $r/R = 0.775$, when the solids concentration is increased. This failure, however, does not seem to affect the model's capability to properly describe the region near the wall and the centerline of the riser. A possible reason may be that during the transition from lean to denser conditions, some parameters of the model may change, for example, the radial dispersion coefficient of the lean phase. In the present study, all parameters concerning the gas mixing have been taken from previous experiments (Kruse et al., 1995), which were carried out under rather dilute operating conditions. Thus, it cannot be expected that the model can account for all phenomena to occur within a very wide range of operating conditions. Current work concerns improvements of the model, with respect to dense conditions.

Under all operating conditions, the radial gradients of the ozone concentration are much higher than the axial gradients. This is especially true in those cases with higher solids concentration. It is remarkable that near the gas distributor extremely low ozone concentrations are found adjacent to the wall, whereas the total conversion is rather low. Obviously, the CFB riser exhibits significant mass transfer limitations, which have to be taken into account. If one considers more rapid reactions than the ozone decomposition, for example,

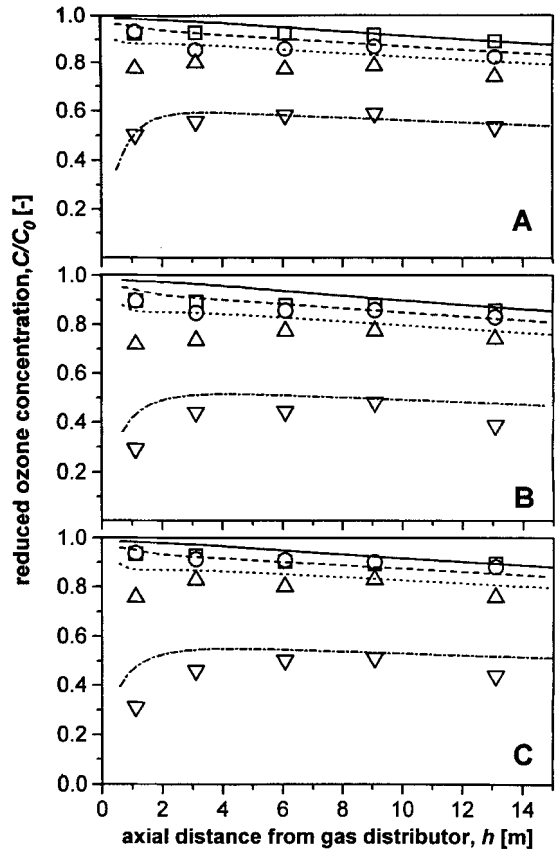

Figure 19. Comparison of measured and calculated ozone concentration profiles for low values of the solids holdup.

Experimental conditions as given in Tables 1 and 3. Symbols: experimental data (□: center, ○: $r/R = 0.6$, Δ: $r/R = 0.775$, ∇: wall). Lines: corresponding model calculations.

combustion of solid fuels, the mass transfer limitations are even more important than in the present study. In the case of combustion processes, one has to be aware of the existence of reducing conditions, because at some locations the oxygen concentrations may drop to values of essentially zero. It can be concluded for catalytic synthesis reactions, that the catalyst efficiency is significantly lowered in the region near the wall of the riser, because the reactant concentration may drop to very low figures. Since a major fraction of the catalyst is in this region, this finding is important for prediction of the reactor performance.

The present model may serve as a useful tool to predict the behavior of CFB reactors that are assumed to be affected by internal mass transfer limitations. At the present state of development, the behavior of a pilot-scale CFB reactor can be properly described on the basis of parameters that were determined from tracer gas experiments only. However, the present approach would benefit from future improvements. The currently used model for the flow structure near the gas distributor is definitely too simple for an appropriate description of the complex phenomena to occur there. Moreover, the results obtained at the radial position of $r/R = 0.775$ indicate that the description of radial gas mixing requires major improvements in the case of high values of the solids holdup. However, there is a good agreement of measurement and cal-

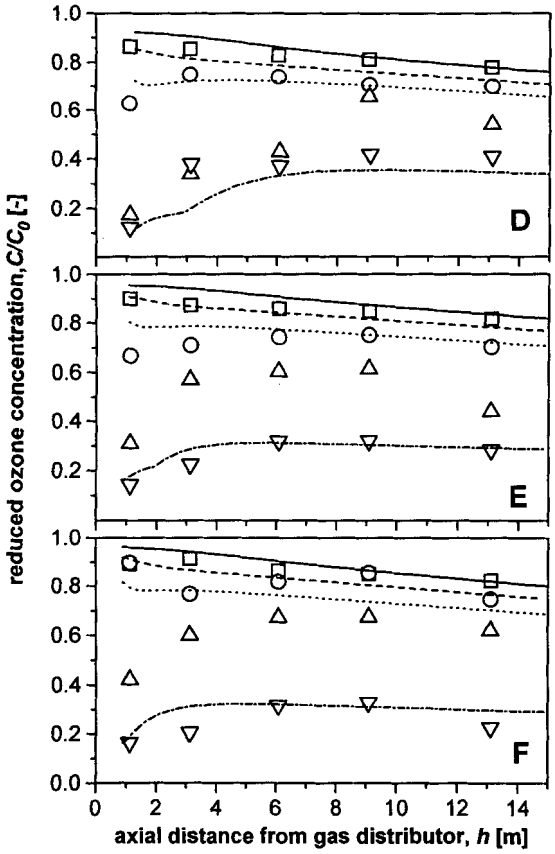

Figure 20. Comparison of measured and calculated ozone concentration profiles for intermediate values of the solids holdup.

Experimental conditions as given in Tables 1 and 3. Symbols: experimental data (□: center, ○: $r/R = 0.6$, Δ: $r/R = 0.775$, ∇: wall). Lines: corresponding model calculations.

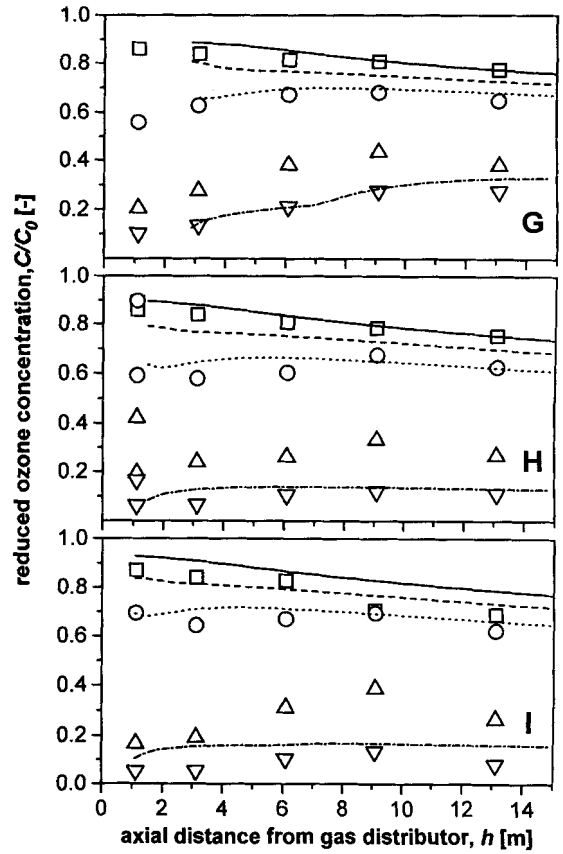

Figure 21. Comparison of measured and calculated ozone concentration profiles for high values of the solids holdup.

Experimental conditions as given in Tables 1 and 3. Symbols: experimental data (□: center, ○: $r/R = 0.6$, Δ: $r/R = 0.775$, ∇: wall). Lines: corresponding model calculations.

culation at the wall and in the center of the riser. Since this agreement has been obtained without any parameter fitting it may be concluded that the present approach offers a high potential for future development.

Conclusions

A two-dimensional model for the description of the reaction behavior of CFB systems has been developed. The approach makes use of an existing gas-mixing model for the upper dilute zone of a CFB reactor. Parameters of the model have been determined from earlier tracer gas experiments. Thus, the model allows us to predict the performance of a CFB reactor, provided the axial distribution of solids and a pair of radial profiles of upward and downward solids mass fluxes are given.

The approach has been evaluated using a model reaction, the ozone decomposition, in a cold model CFB reactor (H_t = 15.6 m, d_t = 0.4 m). The experimental data indicate that the CFB reactor is characterized by significant internal mass transfer limitations causing strong radial concentration gradients of gaseous reactants. This characteristic feature should be taken into consideration when CFB reactors are designed for a specific application. It is shown that the present model is very well able to describe the measurements for the case of low solids holdup. If the solids concentration is higher, the model yields appropriate descriptions of the CFB reactor behavior near the wall and in the center of the riser, whereas at intermediate radial positions deviations occur. However, the results of the study show the high potential of the present modeling approach, which can account for major properties of the CFB reactor. Future improvements should be focused on the behavior of these systems near the gas distributor and on a better description of the flow structure and the radial gas mixing for systems that are operated under dense conditions.

Acknowledgment

Financial support by the Deutsche Forschungsgemeinschaft through Sonderforschungsbereich 238, by Japan's NEDO—New Energy and Industrial Technology Development Organisation—and by the BASF AG is gratefully acknowledged. Moreover, the authors would like to express their thanks to Ralf Goetzinger and Michael Fluegge for their experimental work.

Notation

a = exponential decay constant in Eq. 3, m^{-1}
c_v = local solids volume fraction
c'_v = solids volume fraction at the lower end of the upper dilute zone
$c_{v\infty}$ = solids volume fraction at infinite distance from the gas distributor
d_t = riser diameter, m
g = gravity acceleration, m/s^2

G_s = external solids circulation rate, kg/(m^2·s)
G_{si} = solids circulation rate as calculated from integration of local solids mass flux profiles, kg/(m^2·s)
H_b = height of bottom zone, m
H_t = total height of riser
R = riser radius, m
ρ_s = apparent solids density, kg/m^3

Indices

0 = at the gas distributor
c = convective
w = region in the bottom zone for $r > R_{net}$

Literature Cited

Arena, U., A. Malandrino, and L. Massimilia, "Modeling of Circulating Fluidized Bed Combustion of Char," *Can J. Chem. Eng.*, **69**, 860 (1991).

Basu, P., J. Talukdar, and W. Song, "Experimental Validation of an One and Half Dimensional Model of Char Combustion in a Circulating Fluidized Bed," *AIChE Symp. Ser.*, **301**(90), 114 (1994).

Boemer, A., A. Braun, and U. Renz, "Emissions of N_2O from Four Different Large Scale Circulating Fluidized Bed Combustors," *Proc. Int. Conf. on Fluidized Bed Combustion*, L. N. Rubow, ed., San Diego, p. 585 (1993).

Brereton, C. M. H., J. R. Grace, and J. Yu, "Axial Gas Mixing in a Circulating Fluidized Bed," *Circulating Fluidized Bed Technology II*, P. Basu and J. F. Large, eds., Pergamon Press, New York, p. 307 (1988).

Contractor, R. M., G. S. Patience, D. I. Garnett, H. S. Horowitz, G. M. Sisler, and H. E. Bergna, "A New Process for N-Butane Oxidation to Maleic Anhydride Using a Circulating Fluidized Bed Reactor," *Circulating Fluidized Bed Technology IV*, A. A. Avidan, ed., Pergamon Press, New York, p. 387 (1993).

Edwards, M., and A. Avidan, "Conversion Model Aids Scale-up of Mobil's Fluid Bed MTG Process," *Chem. Eng. Sci.*, **41**, 829 (1986).

Hartge, E.-U., D. Rensner, and J. Werther, "Solids Concentration and Velocity Patterns in Circulating Fluidized Beds," *Circulating Fluidized Bed Technology II*, P. Basu and J. F. Large, eds., Pergamon Press, Oxford, p. 165 (1988).

Horio, M., H. Hatano, M. Ogasawara, M. Kruse, E.-U. Hartge, and J. Werther, "Local Gas and Cluster Velocities in a Large-scale Circulating Fluidized Bed Test Rig," *Chem. Eng. Sci.*, in press (1996).

Kagawa, H., H. Mineo, R. Yamazaki, and K. Yoshida, "A Gas-Solid Contacting Model for Fast Fluidized Bed," *Circulating Fluidized Bed Technology III*, P. Basu, M. Horio, and M. Hasatani, eds., Pergamon Press, New York, p. 551 (1991).

Kruse, M., and J. Werther, "2D Gas and Solids Flow Prediction in Circulating Fluidized Beds Based on Suction Probe and Pressure Profiles Measurements," *Chem. Eng. Proc.*, **34**, 185 (1995).

Kruse, M., H. Schoenfelder, and J. Werther, "A Two-Dimensional Model for Gas Mixing in the Upper Dilute Zone of a Circulating Fluidized Bed," *Can. J. Chem. Eng.*, **73**, 620 (1995).

Kunii, D., and O. Levenspiel, *Fluidization Engineering*, Butterworth-Heinemann, Stoneham, MA, p. 201 (1991).

Lints, M. C., and L. R. Glicksman, "The Structure of Particle Clusters near the Wall of a Circulating Fluidized Bed," AIChE meeting, Orlando, FL (1992).

Luca, M., M. Luigi, and R. Giorgio, "Comparison Among Several Predictive Models for Circulating Fluidized Bed Reactors," Conf. on Fluidization, Tours, France, p. 475 (1995).

Molodtsof, Y., "Hydrodynamics and Heat Transfer to Vertically Flowing Gas-Solids Suspensions," *KONA*, No. 10, p. 41 (1992).

Monceaux, L., M. Azzi, Y. Molodtsof, and J. F. Large, "Overall and Local Characterization of Flow Regimes in a Circulating Fluidized Bed," *Circulating Fluidized Bed Technology*, P. Basu, ed., Pergamon Press, Oxford, p. 185 (1986).

Ouyang, S., X.-G. Lin, and O. E. Potter, "Circulating Fluidized Bed as a Catalytic Reactor: Experimental Study," *AIChE J.*, **41**, 1534 (1995).

Ouyang, S., X.-G. Lin, and O. E. Potter, "Ozone Decomposition in a 0.254 m Diameter Circulating Fluidized Bed Reactor," *Powder Technol.*, **74**, 73 (1993).

Press, W. H., S. A. Teukolsky, W. T. Vetterling, and B. P. Flannery, *Numerical Recipes in FORTRAN: The Art of Scientific Computing*, 2nd ed., Cambridge Univ. Press, Cambridge, England (1992).

Pugsley, T. S., G. S. Patience, F. Berruti, and J. Chaouki, "Modeling the Catalytic Oxidation of n-Butane to Maleic Anhydride in a Circulating Fluidized Bed Reactor," *Ind. Eng. Chem. Res.*, **31**, 2652 (1992).

Rhodes, M. J., X. S. Wang, H. Cheng, T. Hirama, and B. M. Gibbs, "Similar Profiles of Solids Flux in Circulating Fluidized Bed Risers," *Chem. Eng. Sci.*, **47**(7), 1635 (1992).

Richardson, J. F., and W. N. Zaki, "Sedimentation and Fluidization: Part I," *Trans. Inst. Chem. Eng.*, **32**, 34 (1954).

Schoenfelder, H., J. Hinderer, J. Werther, and F. Keil, "Methanol to Olefins—Prediction of the Performance of a Circulating Fluidized Bed Reactor on the Basis of Kinetic Experiments in a Fixed Bed Reactor," *Chem. Eng. Sci.*, **49**(24B), 5377 (1994a).

Schoenfelder, H., J. Werther, J. Hinderer, and F. Keil, "A Multi-Stage Model for the Circulating Fluidized Bed Reactor," AIChE Symposium Series, **301**(90), 92 (1994b).

Tsuo, Y. Y. P., Y. Y. Lee, A. Rainio, and T. Hypanen, "Three Dimensional Modeling of N2O and NOx Emissions from Circulating Fluidized Bed Boilers," *Proc. Int. Conf. on Fluidized Bed Combustion*, K. J. Heinschel, ed., Orlando, FL, p. 1059 (1995).

Van Swaaij, W. P. M., and F. J. Zuiderweg, "Investigation of Ozone Decomposition in Fluidized Beds on the Basis of a Two-Phase Model," *Proc. of the European Symp. on Chemical Reaction Engineering*, Amsterdam, Elsevier, Amsterdam, p. B9-25 (1972).

Van Swaaij, W. P. M., "The Design of Gas-Solid Fluid Bed and Related Reactors," *Chemical Reaction Engineering Review*, D. Luss and V. W. Weekman, Jr., eds., ACS, Washington, DC, p. 329 (1978).

Werther, J., "Fluid Mechanics of Large-Scale CFB Units," *Circulating Fluidized Bed Technology IV*, A. A. Avidan, ed., p. 1 (1993).

Werther, J., T. Ogada, and C. Philippek, "Sewage Sludge Combustion in the Fluidized Bed. Comparison of Stationary and Circulating Fluidized Bed Techniques," *Proc. Int. Conf. on Fluidized Bed Combustion*, K. J. Heinschel, ed., Orlando, FL, p. 951 (1995).

Zhang, W., Y. Tung, and F. Johnsson, "Radial Voidage Profiles in Fast Fluidized Beds of Different Diameters," *Chem. Eng. Sci.*, **46**(12), 3045 (1991).

Manuscript received July 12, 1995, and revision received Oct. 31, 1995.